Journal of Orthopaedic Research

The Effect of Imbalanced Loading on Hip Joint Development and Maturation

SCHOLARONE™
Manuscripts

The Effects of Imbalanced Muscle Loading on Hip Joint Development and Maturation

Caleb A. Ford[1]

Niamh C. Nowlan[2]

Stavros Thomopoulos[1,3]

Megan L Killian[1,4]

[1]Washington University School of Medicine, Department of Orthopedic Surgery, St Louis, Missouri, 63110, USA

[2]Imperial College London, Department of Bioengineering, London SW7 2AZ, UK

[3]Columbia University, Department of Orthopedic Surgery, New York, New York, 10027, USA

[4]University of Delaware, Department of Biomedical Engineering, Newark, Delaware, 19716, USA

Running title: Postnatal muscle imbalance alters hip morphology

Author Contributions Statements: CAF contributed to study design, data collection, data analysis, data interpretation and manuscript preparation. NCN contributed to data analysis, data interpretation, and manuscript preparation. ST contributed to study design and manuscript preparation. MLK contributed to study design, data collection, data analysis, data interpretation and manuscript preparation. All authors have read and approved the final submitted version of the document.

Corresponding author:

Megan L. Killian, PhD

Assistant Professor

University of Delaware

Department of Biomedical Engineering

Newark, Delaware, 19716

killianm@udel.edu

1 **Abstract**:

2 The mechanical loading environment influences the development and maturation of joints. In

3 this study, the influence of imbalanced muscular loading on joint development was studied using

4 localized chemical denervation of hip stabilizing muscle groups in neonatal mice. It was

5 hypothesized that imbalanced muscle loading, targeting either Gluteal muscles or Quadriceps

6 muscles, would lead to bilateral hip joint asymmetry, as measured by acetabular coverage,

7 femoral head volume and bone morphometry, and femoral-acetabular shape. The contralateral

8 hip joints as well as age-matched, uninjected mice were used as controls. Altered bone

9 development was analyzed using micro-computed tomography, histology, and image registration

10 techniques at post-natal days (P) 28, 56, and 120. This study found that unilateral muscle

11 unloading led to reduced acetabular coverage of the femoral head, lower total volume, lower

12 bone volume ratio, and lower mineral density, at all three time points. Histologically, the

13 femoral head was smaller in unloaded hips, with thinner triradiate cartilage at P28 and thinner

14 cortical bone at P120 compared to contralateral hips. Morphological shape changes were evident

15 in unloaded hips at P56. Unloaded hips had lower trabecular thickness and increased trabecular

16 spacing of the femoral head compared to contralateral hips. The present study suggests that

17 decreased muscle loading of the hip leads to altered bone and joint shape and growth during

18 post-natal maturation. Statement of Clinical Significance: Adaptations from altered muscle

19 loading during postnatal growth investigated in this study have implications on developmental

20 hip disorders that result from asymmetric loading, such as patients with limb-length inequality or

21 dysplasia.

22

23   **Introduction**

24   The mechanical loading environment influences the development and maturation of

25   joints.[1-4] For example, adaptations to bone due to increased or decreased muscle loading can

26   influence bone shape and structure in newborns, adolescents, and adults.[5,6] Furthermore, changes

27   to the shape and structure of bones can lead to abnormal joint loading patterns, onset and

28   progression of conditions such as acetabular dysplasia, and increased risk of osteoarthritis (OA).[7]

29   Thus far, the role of early-stage, post-natal muscle unloading on the shape, structure, and

30   function of maturing articular joints is not well understood, particularly for the hip.

31   The hip joint continues to develop and mature during post-natal life and into childhood;

32   e.g., in humans, the triradiate cartilage does not fully ossify until ages 15-18.[8,9] Post-natal muscle

33   loading at the hip is therefore critical for the formation of the proximal femur and acetabulum.

34   Understanding the role of muscle unloading and/or imbalance on hip bone growth and

35   mineralization as well as growth plate fusion (particularly of the triradiate cartilage and proximal

36   femur) will guide our understanding of hip maturation and may provide insight into the

37   progression of developmental hip disorders. In humans, the triradiate cartilage of the hip fuses at

38   the time of skeletal maturity and consists of three distinct growth plates that connect the ilium,

39   ischium, and pubis. These growth plates fuse to form the acetabulum, which is loaded orthogonal

40   to the axis of growth plate fusion.[8] Expansion of the triradiate cartilage during postnatal growth

41   is necessary for proper joint development in humans and this expansion ends when the pelvis has

42   fully ossified.[10] Clinical case reports of premature closure of the triradiate cartilage suggest a

43   causative association with predisposition to the development of acetabular dysplasia, or

44   developmental dysplasia of the hip (DDH).[9,11-14]

45   Postnatal straight-legged swaddling, previously common in Japanese and Native

46   American culture, can lead to DDH in hips that are otherwise healthy at birth, and this is

47   analogous to muscular unloading. This disorder has been replicated in animal models and leads

48   to hip instability and dislocation. Additionally, defective development of the hip joint with

49   conditions, such as DDH, carries a chronic and indolent course of disease. It is estimated that 79-

50   90% of cases of OA have definable, congenital hip joint abnormalities that lead to increased

51   impingement or altered stress loading.[15,16] The influence of altered mechanics on development of

52   OA is likely even greater on development of OA in early adulthood. [17] Center edge angle

53   (corresponding to "Norberg angle") on radiographs early in adult life have been shown to

54   correlate with WOMAC score for symptomatic OA. [18] Understanding causes and preventative

55   measures for OA is critical, as clinical OA is estimated to affect 27 million US adults (10% of

56   those over age 18) and cost 42.3 billion USD annually. [19]

57   Mice undergo a similar hip joint maturation process as humans and other mammals,

58   whereby the hip follows an ordered, triradiate ossification process that converges towards the

59   acetabulum and is completed following a period of postnatal growth.[20] The pelvis emerges

60   during development in mice as a single cartilage template, which then separates into three

61   ossification centers that include the ilium, ischium, and pubis.[20] The proximal femur of mice

62   begins as a single chondroepiphysis at early postnatal growth, and this epiphysis later separates

63   into two epiphyses, one of the greater trochanter and another of the femoral head.[21] The rapid

64   growth of the mouse skeleton is convenient for studying bone and joint maturation, as the

65   separation of the proximal chondroepiphysis of the femur occurs in the first 4 weeks of postnatal

66   growth,[22] and fusion of the triradiate cartilage in the acetabulum occurs within the first 3 months

67   of postnatal growth. The use of mouse models to study musculoskeletal growth and response to

68   mechanical unloading is particularly beneficial, as mice are genetically similar to humans, have a

69   relatively fast rate of postnatal maturation, and offer a number of available genetically modified

70   tools compared to other mammalian research species.

71   Recent work using embryonic culture of chick has shown that neonatal muscle loading

72   influences the development of the embryonic hip joint.[23] This study suggested that prenatal

73   immobilization of the embryonic hip, induced by spinal muscle atrophy, may induce early-onset

74   DDH.[23] However, this study was unable to explore the postnatal adaptations of the hip following

75   muscle unloading due to the global impact of muscle immobilization in the model used.[23]

76   Therefore, assessing the postnatal joint morphology following localized muscle unloading is

77   needed. In the present study, it was hypothesized that unilateral muscular unloading (i.e.,

78   unbalanced loading) via localized denervation of hip flexors (e.g., lateral quadriceps) or hip

79   extensors (e.g., gluteus maximus) would lead to structural and functional alterations of the hip

80   during post-natal maturation. An *in vivo* model of unilateral muscle unloading of hip stabilizers

81   was developed in neonatal mice to identify the role of muscle loading on hip development during

82   post-natal growth. Acetabular coverage, femoral head volume, histomorphology, and bone

83   morphometry were examined to detect differences between unloaded and contralateral hips.

84   **Methods**

85   *Unilateral hip unloading model*

86   All studies were performed in compliance with the Animal Studies Committee and the

87   Department of Comparative Medicine at Washington University. CD-1 neonatal mice (post-natal

88   day 1, P1, N = 56) were administered intramuscular injections of 0.15-0.2U botulinum toxin A

89   (BOTOX; Allergan, Inc.) in saline in the left hips (N = 3-10 per group/time point), with an

90   equivolumetric dose of 0.9% saline in the contralateral hip. Botox was used to paralyze the

91   injected muscles during post-natal growth[22]. Mice were injected in the lateral aspect of their

92   upper thigh (Quad target) or the caudal aspect of the gluteus muscle groups (Gluteal target) twice

93   weekly until weaning and once per week thereafter until sacrifice at P28 and P56. Injections

94   were made with a 28 gauge, 0.3mL total volume insulin syringe (Becton Dickinson and

95   Company, Franklin Lakes, NJ) and the needle was oriented as follows: for Quad target, the pup

96   was held gently by its scruff with its hindlimb in full extension. Following palpation of the thigh,

97   the needle was inserted subcutaneously and into the muscle belly of the rectus femoris, parallel

98   to the direction of muscle action, near the patellar tendon. For Gluteal target, the pups' hindlimbs

99   were secured between the handler's thumb and middle finger after placing the pup with its

100   ventral side on the handler's index finger. The hip bone and musculature was palpated to identify

101   the gluteus maximus muscles and the needle was aligned parallel to the action line of the muscle

102   and inserted subcutaneously into the muscle belly. An additional group for Gluteal target

103   unloading only was carried out through P120. Uninjected litters were used as age-matched

104   controls for P28 and P56 time-points (5-6 per time point, N = 11 total). Mice were housed with

105   their mothers until wean (P21) and then housed with same-sex littermates in a barrier facility

106   with 12hr on/12 hr off light cycle. Mice were monitored for distress throughout the duration of

107   the experiment. Mice were euthanized via carbon dioxide asphyxiation. Following sacrifice, their

108   intact hips with surrounding musculature were immediately dissected and fixed in hip extension

109   position using 4% paraformaldehyde.

110   *Hip unloading with recovery model*

111   A fourth group of mice (N = 7) were injected as previously described for Glute target unloading.

112   At P14, a subset of these mice ceased unilateral Botox treatment and began bilateral saline

113   injections in an effort to encourage unloading recover (Recovery group, N = 4) while the

114   remaining mice were chronically injected (Maintained Unloading group, N = 3) as described in

115   the unloading model. At P56, hips of Recovery and Maintained Unloading groups were dissected

116   as previously described and fixed in 4% paraformaldehyde in an anatomical position with the

117   hips held slightly abducted and flexed.

118   *Microcomputed tomography and histology*

119   Following fixation, P28 and P56 control, Gluteal target unloading, and Quad target

120   unloading hips were scanned using micro-computed tomography (μCT, standard resolution,

121   36μm voxel, 45kVp, 177μA, and 250msec integration time; Scanco μCT40, Switzerland). μCT

122   scans were exported as DICOM files and analyzed in OsiriX 32-bit freeware (Pixmeo SARL,

123   Bernex, Switzerland). Hips were digitally repositioned, oriented in craniocaudal plane, and

124   aligned using the 3D MPR tool in OsiriX. Norberg angles (α, angle of Weiberg + 90°, Figure

125   1A) for each animal's right and left hips were measured using tools in the 3D MPR tool on at

126   least 5 consecutive slices. Total volume (TV), bone volume (BV), bone volume percentage

127   (BV/TV), and total mineral density (TMD, mg HA/cm^3) of the femoral head was analyzed using

128   Scanco software. High resolution scans were obtained for Recovery and Maintained Unloading

129   groups, as well as P120 control and Gluteal Target hips (high resolution setting, 20μm voxel,

130   45kVP, 177μA) for TMD, bone mineral density (BMD), trabecular thickness (Tb.Th.), spacing

131   (Tb.Sp.), and number (Tb.N.). Following μCT, samples were decalcified in 14% EDTA and

132   processed for paraffin embedding and histology. Histological sections were cut at 7μm thick

133   sections for both left and right hips of Quad Target (P28 only), Gluteal Target (P28, P56, and

134   P120), and controls (P28 and P56) and stained using toluidine blue.

135   *Image registration and shape comparisons*

136   Image registration was performed using the Image Registration Toolkit (IRTK, since

137 upgraded to MIRTK https://biomedia.doc.ic.ac.uk/software/mirtk/, last accessed March 2016)[24].

138 Data from both left and right hips at P56 and P120 (P56 control, P56 Gluteal Target, P120

139 control, and P120 Gluteal Target) were included for image registration. For each specimen, both

140 left and right proximal femur and acetabular region of the pelvis were virtually segmented using

141 Mimics (Materialise, Belgium) in preparation for image registration. All right-sided femora and

142 pelvises were mirrored to enable comparison with the contralateral counterparts. Within each

143 group, multiple rigid registrations and transformations were performed to align all femora or

144 pelvises in the group in exactly the same orientation and position. Next, an atlas image was

145 created to provide an average of the aligned input images, thereby providing an average

146 representation of the shape for the left or right side of that treatment group. Within each group

147 (e.g., P120 Gluteal Target), four atlases were created; left femur, right femur, left pelvis and right

148 pelvis. The left and right atlases of the same rudiments within each group were then aligned with

149 respect to each other using a further iteration of rigid registration and transformation. Each atlas

150 was thresholded (using the same parameters within each comparison set) in order to remove

151 noise due to sub-optimal alignment of a minority of datasets, or due to shapes that are

152 significantly different from the standard shape for that particular group. Finally, ImageJ

153 (http://rsbweb.nih.gov/ij/, last accessed March 2016)[25] was used to calculate the pixel differences

154 between each set of atlases, with the output of this step demonstrating region specific size and

155 shape differences between the left and right sides for all groups.

156 *Statistical Analysis*

157 All statistical comparisons were performed using Prism 6 (version 6.0d, Graphpad). 2-way

158 ANOVA with Holm-Sidak multiple comparisons tests ($1 - \beta = 0.80$; $\alpha = 0.05$) were used to

159   compare Norberg angles, TV, BV, BV/TV, and TMD for control, Quad Target and Gluteal

160   Target animals at P28 and P56 time points with repeated measures (left and right limbs paired).

161   Linear regression was performed to test goodness of fit and to compare slopes and intercepts that

162   describe the relationship between Norberg angle (α) and bone morphometric outcomes (TV,

163   BV/TV, and TMD) for Gluteal-target Unloaded and Contralateral groups as well as for combined

164   Gluteal-target Unloaded/Contralateral data (P28 and P56 combined; $\alpha = 0.05$). For trabecular

165   outcomes at P120 (Unloaded/Contralateral), paired t-tests were used to compare total volume,

166   BV/TV, and TMD of the trabecular bone of the femoral head, as well as trabecular thickness

167   (TbTh), number (TbN), and spacing (TbSp) of the Contralateral and Unloaded hips ($\alpha = 0.05$).

168   For trabecular outcomes at P56 for the Recovery and Maintained Unloading groups, 2-way

169   ANOVA with repeated measures was used to compare left vs. right proximal femur bone

170   morphometry (TV, BV, BV/TV, TMD, TbSp, TbN, and TbTh) between Recovery and

171   Maintained Unloading groups ($\alpha = 0.05$).

172   **Results**

173   All animals responded well to the injections and were used in analyses. Post-natal

174   imbalanced loading via isolated paralysis of either the the hip flexors (i.e., quadriceps) or hip

175   extensors/stabilizers (i.e., gluteus maximus) led to a decreased Norberg angle at P28 and P56

176   compared to the contralateral side (Figure 1B). No statistical differences in Norberg angle were

177   found between the contralateral limb and uninjected, age-matched controls at P28 or P56.

178   Norberg angle did not differ between left and right femoro-acetabular joints for control hips

179   (Figure 1B).

180   Hips that developed with imbalanced loading had significantly smaller TV (Figure 2A)

181   and reduced TMD (Figure 2E) compared to their contralateral sides, for both Quad and Gluteal

182   target groups, at both P28 and P56. No statistical differences were observed between Gluteal

183   Target unloading and contralateral data using linear regression (Figure 2B); however, after

184   Gluteal Target unloaded and contralateral data were pooled for linear regression, there was a

185   significant relationship between TV and Norberg angle ($R^2 = 0.3471$, p < 0.001; Figure 2B).

186   BV/TV was significantly lower in femoral heads from unloaded hips compared to contralateral

187   hips at P28; however, BV/TV was only significantly lower in unloaded hips compared to

188   contralateral hips at P56 for the Gluteal target group (Figure 2C). A significant linear

189   relationship was observed between BV/TV and Norberg angle for unloaded, but not

190   contralateral, hips ($R^2 = 0.6351$, p < 0.0001; Figure 2D). Pooled BV/TV and Norberg angle

191   comparisons using linear regression was statistically significant ($R^2 = 0.2139$, p = 0.0045; Figure

192   2D). TMD of the proximal femur was significantly lower for Gluteal target and Quad target,

193   compared to contralateral hips, at P28 and P56 (Figure 2E). A significant linear relationship was

194   observed between TMD and Norberg angle for unloaded hips ($R^2 = 0.6428$, p < 0.001; Figure

195   2F), but not contralateral hips (Figure 2F). Pooled TMD and Norberg angle comparisons using

196   linear regression was statistically significant ($R^2 = 0.2295$, p = 0.0031; Figure 2F). No statistical

197   differences were found between the contralateral limb and uninjected, age-matched controls for

198   TV, BV/TV, or TMD at P28 or P56. However, BV/TV and TMD significantly increased from

199   P28 to P56 for all groups (Figure 2C & E). Femoral head TV, BV/TV, and TMD did not vary

200   between left and right control hips at either P28 or P56 (Figure 2).

201   The trabecular structure of the femoral head was examined in contralateral and unloaded

202   hips at P56 and P120 (Figure 3). Trabecular bone adaptations included decreased trabecular

203   volume in the femoral head (Figure 3A), consistent with observations at earlier time points when

204   including the cortical bone in the analysis (Figure 2A). Similarly, trabecular BV/TV and TMD

205   were significantly lower in unloaded femoral heads compared to contralateral femoral heads at

206   P120 (Figure 3B & C). Trabecular thickness (TbTh) was significantly reduced (Figure 3D) and

207   TbSp was significantly increased (Figure 3F) for unloaded hips compared to contralateral hips.

208   The number of trabeculae (TbN) did not differ significantly between groups at this time point

209   (Figure 3E).

210   In mice that were allowed to recovery during postnatal growth after an unloading period

211   of 2 weeks, the trabecular/bone morphometry were significantly different than hips from age-

212   matched littermates receiving Maintained Unloading (Figure 4). Specifically, TMD and BV/TV

213   were significantly higher in both Contralateral and short-term Unloaded hips following a period

214   of recovery compared to the Contralateral and Unloaded hips of age-matched littermates that

215   received Maintained Unloading during postnatal growth (Figure 4C & D). A period of recovery

216   also resulted in decreased TbSp and increased TbTh compared to Maintained Unloading for

217   unloaded limbs (Figure 4A & B).

218   Shape differences between right (contralateral) and left (unloaded) hips were visualized

219   between thresholded atlases of rigidly registered datasets (Figure 5). Color mapping and pixel

220   density indicates shape differences between the groups; magenta indicates that more growth

221   occurred in that region for the right (contralateral) bone whereas turquoise indicates that more

222   growth occurred in that region for the left (unloaded) bone. Control hips at P56 are shown in

223   Figure 5A, C, & E, and the Gluteal-target hips are shown in Figure 5B, D, and F. For control

224   hips, there are mild or no differences in growth patterning between left and right hips, as

225   indicated by the amount of white pixels (e.g., matching size). However, for the Gluteal-target

226   hips, the contralateral acetabulum was markedly larger compared to the unloaded acetabulum

227   (Figure 5B). The greater and lesser trochanter, as well as the medial, articulating surface of the

228   femoral head, were larger in the contralateral hip compared to the unloaded hip, indicated by

229   more magenta patterning on these surfaces (Figure 5D). Surprisingly, the proximal surface of the

230   femoral head as well as the proximal femoral neck displayed more pronounced outgrowths in the

231   unloaded group compared to the contralateral group, indicated by more turquoise patterning on

232   this surface (Figure 5F).

233   At all three time points, the histology of the hip joint reflected the shape adaptions in

234   femoral head following imbalanced loading (Figure 6, top row). At P28, the femoral head

235   appeared smaller than the contralateral control following Quad-target unloading (Figure 6). The

236   triradiate cartilage of the pelvis, along with its adjacent trabeculae, appeared thinner on the

237   unloaded size compared to the contralateral side (Figure 6, top row). At P56, the triradiate

238   cartilage was fused for both contralateral and unloaded sides, and the femoral head of the

239   unloaded side appeared consistently smaller (Figure 6, middle row). Additionally, at P56, the

240   cartilaginous secondary ossification zone of the femoral head was not yet fully mineralized in all

241   contralateral hips; however, the femoral head had mostly mineralized its secondary ossification

242   center in the unloaded hips (Figure 6, middle row). At P120, the femoral head of the contralateral

243   hip was fully mineralized and mature, with thick subchondral/cortical bone and thickened

244   trabeculae (Figure 6, bottom row). The femoral head of the unloaded hip, however, was less

245   densely mineralized, had thinner trabeculae, and thinner subchondral/cortical bone (Figure 6,

246   bottom row). Similar to the P28 and P56 unloaded hips, the P120 unloaded hips were smaller

247   than their contralateral hips (Figure 6, bottom row).

248   **Discussion**

249   Unilateral postnatal unloading of key hip-stabilizing muscle groups led to decreased

250   acetabular coverage (indicated by decreased Norberg angles), decreased bone accumulation of

251   the femoral head (indicated by decreased TMD), and altered size and shape of the unloaded hip

252   compared to contralateral hips. These changes demonstrate the importance of bilateral dynamic

253   and balanced loading during post-natal maturation of the hip joint for proper joint development.

254   Unilateral adaptations of bone and joints during post-natal growth can have a dramatic

255   impact on the long-term health of bones and joints into adulthood. Recently, femoral head

256   volume has been negatively correlated with cephalad displacement of the femoral head.[26]

257   Unilateral vascular insufficiency has also been correlated with increased risk of femoral neck and

258   acetabular deformities at maturation.[27] Additionally, medial bowing and premature fusion of the

259   femoral physis have been associated with poor outcomes following maturation of the hip in cases

260   of congenital dislocation.[27] The diameter of the acetabulum is controlled by the expansion of

261   triradiate cartilage,[8] and the depth of the acetabulum is controlled by pressures from the femoral

262   head.[28] Premature, unilateral closure and smaller hips may lead to altered gait and degenerative

263   outcomes.[7,10,11] Conversely, asymmetric growth plate expansion of murine long bones of the

264   hindlimb has been shown to be modulated by the delivery of heat, which led to limb length

265   discrepancy and the potential for altered loading patterns between left and right hips.[29]

266   Adaptations to loading during post-natal growth may influence proliferation and differentiation

267   of growth plate cells[29], particularly of the triradiate cartilage and proximal femur, and future

268   work should explore this further.

269   Shape differences between unloaded and contralateral hips may provide insight into the

270   contact areas between the acetabulum and femoral head during stages of linear growth and,

271   concomitantly, following unloading. Because the acetabulum serves as the articulating point of

272   the pelvis and femur, the acetabulum adapts during growth to both constrain the femoral head

273   within the socket but also allow full range of motion without impingement. Increasing coverage

274   of the femoral head by the acetabulum likely leads to increased stability of the joint. It was

275   hypothesized in the study that acetabular coverage would decrease following muscle unloading.

276   We found that there were regions of significant loss of acetabular coverage as a result of

277   unloading, which were in line with changes in the shape of the proximal femur. This study

278   demonstrated that changes in muscular loading of hip stabilizers likely leads to altered contact

279   mechanics of the proximal femur and acetabulum.

280   Results from long term paralysis (P120) validated the results from earlier time points in

281   this study, and also allowed for more detailed analysis of trabecular morphology. The analysis of

282   trabeculae was not performed at earlier time points for a few reasons. At P28, trabeculae were

283   not yet established in the femoral head and therefore trabecular morphology was not determined.

284   Likewise, high variability existed at P56, with some hips showing full, bilateral mineralization of

285   the femoral head and others showing incomplete fusion of the secondary ossification center (as

286   shown in Figure 3). MicroCT images, capable of discerning gross differences in bone

287   mineralization and shape, were obtained at a lower resolution for P28 and P56 compared to

288   P120. At P120, mice had fully mature, mineralized bones, allowing for full characterization of

289   trabecular morphology.

290   Limitations to this study include the use of a contralateral limb as an animal-matched

291   control. Using internal controls increased the statistical power and negated the environmental

292   factors that can affect joint maturation. However, it is likely that localized paralysis affects

293   influenced the animals' overall behavior, potentially altering the development of the contralateral

294   limb. Additionally, the differences between contralateral and unloaded hips may be exacerbated

295   because of the potential compensatory loading of the contralateral hip. This compensatory effect

296   may have been the reason for differences between trabecular bone morphometry in littermate

297   mice that had maintained unilateral unloading and mice that were allowed to recovery from

298   unloading after 2 weeks post-natal. Despite this limitation, the contralateral hips did not differ

299   statistically from the age-matched control hips. It is possible that altered post-natal development

300   has lasting effects that may serve as a model for poor joint loading and subsequent arthritic

301   disease states, such as OA. Our experiments using a period of unloading during early postnatal

302   growth, followed by a period of recovery, showed that the mineralization of the proximal femur

303   is able to recover from short-term periods of unloading. Although we only had a small sample

304   size, these findings are encouraging for understanding the ability of the hip to recovery from a

305   short-term period of unloading during postnatal growth. In an elaborate study of recovery

306   exploring the long-term effects of Botox on shoulder girdle development, Potter et al. found that

307   short-term supraspinatus denervation induced altered shoulder joint maturation and led to

308   protracted bony defects with limited recovery potential.[30] It is likely that growth rates and

309   development of the shoulder and hip girdle follow different time courses, and further studies are

310   necessary to determine the long-term significance of impaired neonatal development on the adult

311   mice after cessation of Botox treatments. Another potential limitation to this study is the risk for

312   targeting the gluteus medius in addition to the gluteus maximus, which could influence abduction

313   of the hip in addition to extension. Future work could involve more careful, microinjection

314   targeting for abductor (gluteus medius) denervation, which could potentially enhance the effects

315   of hip dysplasia.

316   Adaptations in growth and function of hip joint structures play a role in the predisposition

317   to hip OA through altered mechanics and increased local stress.[15,16] Understanding the

318   consequences of post-natal muscle imbalances on hip maturation may provide insight into proper

319   hip development and function. This study investigated the morphological adaptations of the hip

320   in mice subjected to unilateral hip muscle unloading. We found that sustained hip muscle

321   unloading can impair growth and maturation of the femoro-acetabular joint. These findings shed

322   light into the potential perturbation of postnatal musculoskeletal growth patterns driven by

323   muscle imbalance that can influence joint alignment and loading. While not directly investigated

324   in this study, it is possible that altered alignment and loading of the hip likely has long term

325   ramifications for hip joint health and warrants further investigation. There is a rising burden of

326   hip and knee OA in young adults of which etiology is poorly understood, and this increased

327   onset of OA at a young age can lead to an increased social and economic impact on the general

328   population. Therefore, improving our understanding of hip joint growth and maturation in the

329   young adult skeleton may lead to improved rehabilitation strategies and therapeutics that can go

330   beyond total joint arthroplasty or improve implant longevity.

331
332   **Acknowledgements**:

339

340

341

342   **Figure legends**:

343   Figure 1. (A) Representative bilateral measurement of Norberg angles (α) from reoriented,

344   frontal plane microCT image stacks. (B) Norberg angle measurements at P28 and P56 for

345   control, Gluteal-target, and, Quad-target unloading for right (contralateral) and left (unloaded)

346   hips. Solid line indicates significant differences between groups ($p < 0.05$).

347   Figure 2. Bone morphometric outcomes of P28 and P56 control, Gluteal-target, and Quad-target

348   groups of the right (contralateral) and left (unloaded) hips. (A) Total volume (mm^3) of the

349   proximal femur for right and left hips, with (B) linear relationship between Norberg angle (α)

350   and total volume (mm^3) of Unloaded (gray dots) and Contralateral (black dots) Gluteal-targeted

351   proximal femurs. (C) Bone volume ratio (BV/TV), and (D) tissue mineral density (TMD) was

352   measured for the femoral head/neck using microCT. Solid line in A, C, and D indicates

353   significant differences between groups ($p < 0.05$). Solid and dotted black line in B represents the

354   linear correlation for combined Unloaded and Contralateral hips; Respective solid and dotted

355   gray (Unloaded) and black (Contralateral) lines in D and E represent the linear correlation and

356   95% confidence intervals for BV/TV and TMD of Gluteal Unloaded and Contralateral hips,

357   respectively.

358   Figure 3. Trabecular bone morphometry of P120 femoral heads for Gluteal-target contralateral

359   and unloaded hips. (A) Total volume of the trabecular bone in the femoral head (mm^3), (B)

360   BV/TV, (C) tissue mineral density (TMD), and (D-E) trabecular parameters, i.e., thickness

361   (TbTh), number (TbN), and spacing (TbSp), respectively, were compared between contralateral

362   and unloaded groups. Solid bar indicates significant difference between groups ($p < 0.05$).

363   Figure 4. Recovery of bone morphometry after 2 weeks of postnatal Gluteal-target unloading,

364   compared to Maintained Unloading, at P56. (A) TbSp was significantly lower and (B) TbTh was

365   significantly higher for hips that were allowed to recover from postnatal unloading compared to

366   Maintained Unloading. (C and D) Contralateral and Unloaded hips demonstrated higher BV/TV

367   and TMD following a period of Recovery compared to Maintained Unloading. Bar indicates

368   significant difference between group (p < 0.05).

369   Figure 5. Shape comparisons using image registered atlases from microCT images of the (A &

370   B) acetabulum, (C & D) posterior view of the proximal femur, and (E & F) anterior view of the

371   proximal femur at P56. Right (magenta) and Left (turquoise) control hip overlay registrations are

372   shown in A, C, and E; Contralateral (magenta) and Unloaded (turquoise) hip overlay

373   registrations are shown in B, D, and F. Magenta pixels show localization where the

374   contralateral/right atlas is larger, whereas turquoise pixels represent localization of a larger

375   unloaded/left atlas.

376   Figure 6. Histological sections stained with toluidine blue for P28, P56, and P120 contralateral

377   and unloaded hips from the Gluteal-target group. Note the reduced femoral head size for the

378   unloaded group at all 3 time points. Additionally, thickness of the triradiate cartilage is smaller

379   for P28 unloaded hips compared to contralateral hips, and fusion of the femoral physis is

380   accelerated for P56 unloaded hips compared to contralateral hips. Scale bar = 500μm.

381

382

383   **References**

384   1   Drachman, D. & Sokoloff, L. The role of movement in embryonic joint development.

385   *Developmental Biology* 14, 401-420 (1966).

386   2   Giorgi, M., Carriero, A., Shefelbine, S. & Nowlan, N. Effects of normal and abnormal

387   loading conditions on morphogenesis of the prenatal hip joint: application to hip

388   dysplasia. *Journal of Biomechanics* 48, 3390-3397 (2015).

389   3   Giorgi, M., Carriero, A., Shefelbine, S. & Nowlan, N. Mechanobiological simulations of

390   prenatal joint morphogenesis. *Journal of Biomechanics* 47, 989-995 (2014).

391   4   Carter, D., Orr, T., Fyhrie, D. & Schurman, D. Influences of mechanical stress on

392   prenatal and postnatal skeletal development. *Clinical Orthopaedics and Related Research*

393   219, 237-250 (1987).

394   5   Sharir, A., Stern, T., Rot, C., Shahar, R. & Zelzer, E. Muscle force regulates bone

395   shaping for optimal load-bearing capacity during embryogenesis. *Development* 138,

396   3247-3259, doi:10.1242/dev.063768 (2011).

397   6   Burr, D. Muscle strength, bone mass, and age-related bone loss. *Journal of Bone and*

398   *Mineral Research* 12, 1547-1551 (1997).

399   7   Bullough, P. The role of joint architecture in the etiology of arthritis. *Osteoarthritis and*

400   *Cartilage* 12, 2-9 (2004).

401   8   Ponsetti, I. Growth and development of the acetabulum in the normal child. *Journal of*

402   *Bone & Joint Surgery* 60-A, 575-585 (1978).

403   9   Hallel, T. & Salvati, E. Premature clousre of the triradiate cartilage: A case report and

404   animal experiment. *Clinical Orthopaedics and Related Research* 124, 278-281 (1977).

405   10   Gepstein, R., Weiss, R. & Hallel, T. Acetabular dysplasia and hip dislocation after

406   selective premature fusion of the triradiate cartilage. *Journal of Bone and Joint Surgery*

407   66-B, 334-336 (1984).

408   11   Blair, W. & Hanson, C. Traumatic closure of the triradiate cartilage: report of a case.

409   *Journal of Bone & Joint Surgery* 61, 144-145 (1979).

410   12   Bucholz, R., Ezaki, M. & Ogden, J. Injury to the acetabular triradiate physeal cartilage.

411   *Journal of Bone & Joint Surgery* 64, 600-609 (1982).

412   13   Heeg, M., Visser, J. & Oostvogel, H. Injuries of the acetabular triradiate cartilage and

413   sacroiliac joint. *The Bone and Joint Journal* 70, 34-37 (1988).

414   14   Badina, A., Vialle, R., Fitoussi, F. & Damsin, J. Case Reports: Treatment of traumatic

415   triradiate cartilage epiphysiodesis: What is the role of bridge resection? *Clinical*

416   *Orthopaedics and Related Research* 471, 3701-3705 (2013).

417   15   Harris, W. Etiology of osteoarthritis of the hip. *Clinical Orthopaedics and Related*

418   *Research* 213, 20-33 (1986).

419   16   Ganz, R., Leunig, M., Leunig-Ganz, K. & Harris, W. The etiology of osteoarthritis of the

420   hip. *Clinical Orthopaedics and Related Research* 466, 264-272 (2008).

421   17   Lievense, A., Bierma-Zeinstra, S., Verhagen, A., Verhaar, J. & Koes, B. Influence of hip

422   dysplasia on the development of osteoarthritis of the hip. *Annals of Rheumatic Diseases*

423   63, 621-626 (2004).

424   18   Mavcic, B., Iglic, A., Kralj-Iglic, V., Brand, R. & Vengust, R. Cumulative hip contact

425   stress predicts osteoarthritis in DDH. *Clinical Orthopaedics and Related Research* 466,

426   884-891 (2008).

427   19   Murphy, L. & Helmick, C. The impact of osteoarthritis in the United States: A

428   population-health perspective. *American Journal of Nursing* 112, S13-S19 (2012).

429   20   Pomikal, C., & Streicher, J. 4D-analysis of early pelvic girdle development in the mouse

430   (Mus musculus). *Journal of Morphology* 271, 116-126 (2010).

431   21   Serrat, M.A., Reno, P.L., McCollum, M.A., Meindl, R.S., & Lovejoy, C.O. Variation in

432   mammalian proximal femoral development: comparative analysis of two distinct

433   ossification patterns. *Journal of Anatomy* 210, 249-258 (2007).

434   22   Huang, W., Foster, J. & Rogachefsky, A. Pharmacology of botulinum toxin. *Journal of

435   the American Academy of Dermatology* 43, 249-259 (2000).

436   23   Nowlan, N.C., Chandaria, V., & Sharpe, J. Immobilized chicks as a model system for

437   early-onset developmental dysplasia of the hip, *Journal of Orthopaedic Research*, 32,

438   777-785.

439   24   Studholme, C., Hill, D.L.G., & Hawkes, D.J. An overlap invariant entropy measure of 3D

440   medical image alignment, *Pattern Recognition*, 32, 71-86 (1999).

441   25   Abràmoff, M. D., Magalhães, P. J. & Ram, S. J. Image processing with ImageJ.

442   *Biophotonics International* 11, 36-42 (2004).

443   26   Fukiage, K., Fukuda, A., Harada, Y., Suzuki, S., & Futami, T. Femoral head volume

444   indicates the severity of developmental dysplasia of the hip by a method using three-

445   dimensional magnetic resonance imaging. *Journal of Pediatric Orthopaedics* B 24, 286-

446   290 (2015).

447   27   Keret, D., & MacEwen, G.D. Growth disturbance of the proximal part of the femur after

448   treatment for congenital dislocation of the hip. *Journal of Bone and Joint Surgery

449   Am*, 73: 410 -423 (1991).

450   28   Harrison, T.J. The influence of the femoral head on pelvic growth and acetabular form in

451   the rat. *Journal of Anatomy* 95, 12-24 (1961).

452   29   Serrat, M.A., Schlierf, T.J., Efaw, M.L., Shuler, F.D., Godby, J., Stanko, L.M., &

453   Tamski, H.L. Unilateral heat accelerates bone elongation and lengthens extremities of

454   growing mice. *Journal of Orthopaedic Research* 33, 692-698 (2015).

455   30   Potter, R., Havlioglu, N. & Thomopoulos, S. The developing shoulder has a limited

456   capacity to recover after a short duration of neonatal paralysis. *Journal of Biomechanics*

457   47, 2314-2320 (2014).

458
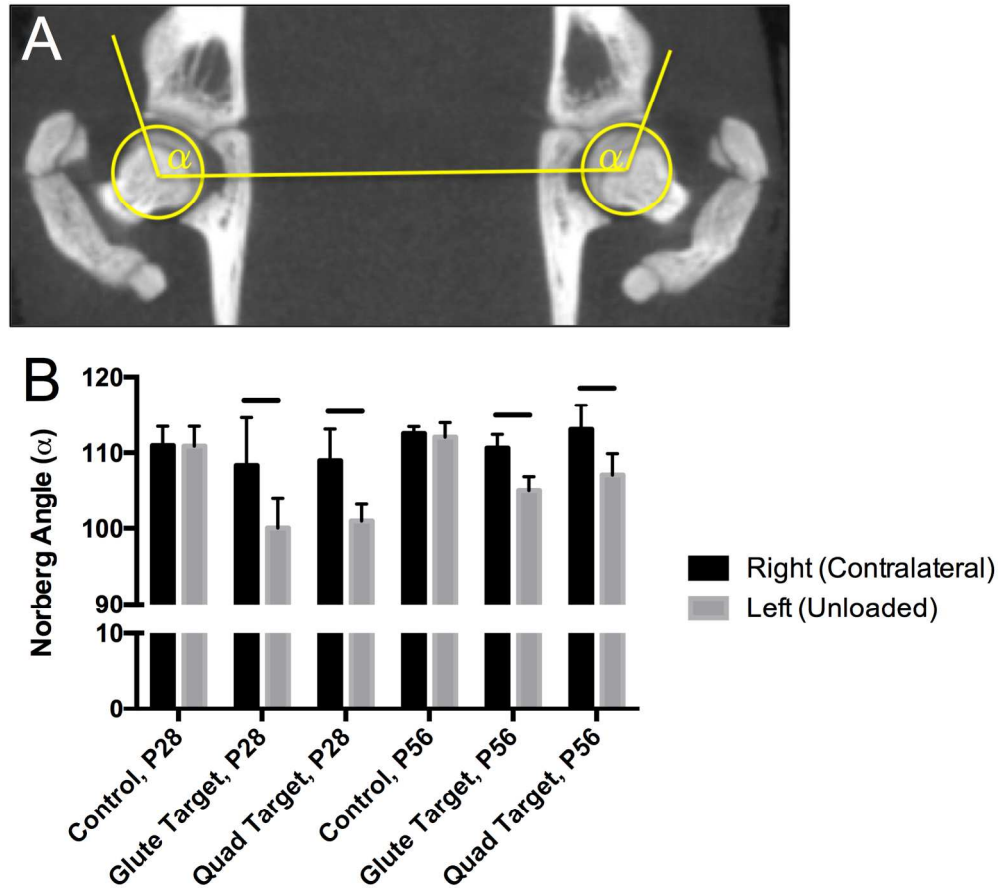
Figure 1. (A) Representative bilateral measurement of Norberg angles (α) from reoriented, frontal plane microCT image stacks. (B) Norberg angle measurements at P28 and P56 for control, Glute-target, and, Quad-target unloading for right (contralateral) and left (unloaded) hips. Solid line indicates significant differences between groups (p < 0.05).
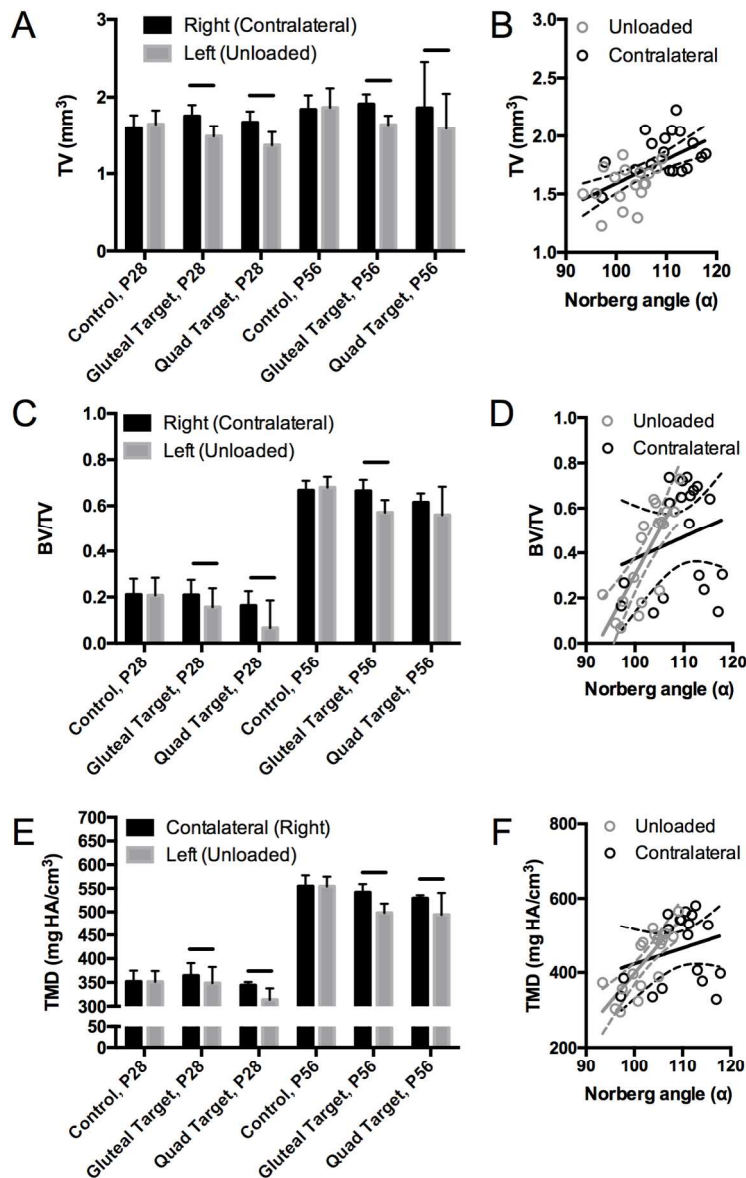431x391mm (144 x 144 DPI)

Figure 2. Bone morphometric outcomes of P28 and P56 control, Gluteal-target, and Quad-target groups of the right (contralateral) and left (unloaded) hips. (A) Total volume (mm3) of the proximal femur for right and left hips, with (B) linear relationship between Norberg angle (α) and total volume (mm3) of Unloaded (gray dots) and Contralateral (black dots) Gluteal-targeted proximal femurs. (C) Bone volume ratio (BV/TV), and (D) tissue mineral density (TMD) was measured for the femoral head/neck using microCT. Solid line in A, C, and D indicates significant differences between groups ($p < 0.05$). Solid and dotted black line in B represents the linear correlation for combined Unloaded and Contralateral hips; Respective solid and dotted gray (Unloaded) and black (Contralateral) lines in D and E represent the linear correlation and 95% confidence intervals for BV/TV and TMD of Gluteal Unloaded and Contralateral hips, respectively.
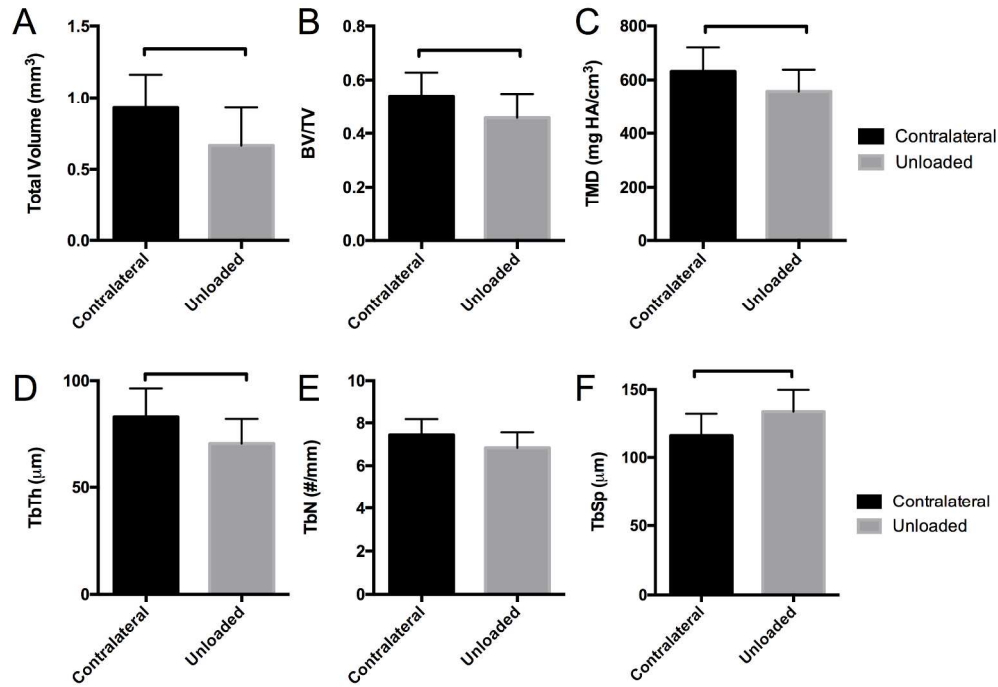253x391mm (144 x 144 DPI)

Figure 3. Trabecular bone morphometry of P120 femoral heads for Gluteal-target contralateral and unloaded hips. (A) Total volume of the trabecular bone in the femoral head (mm3), (B) BV/TV, (C) tissue mineral density (TMD), and (D-E) trabecular parameters, i.e., thickness (TbTh), number (TbN), and spacing (TbSp), respectively, were compared between contralateral and unloaded groups. Solid bar indicates significant difference between groups (p < 0.05).
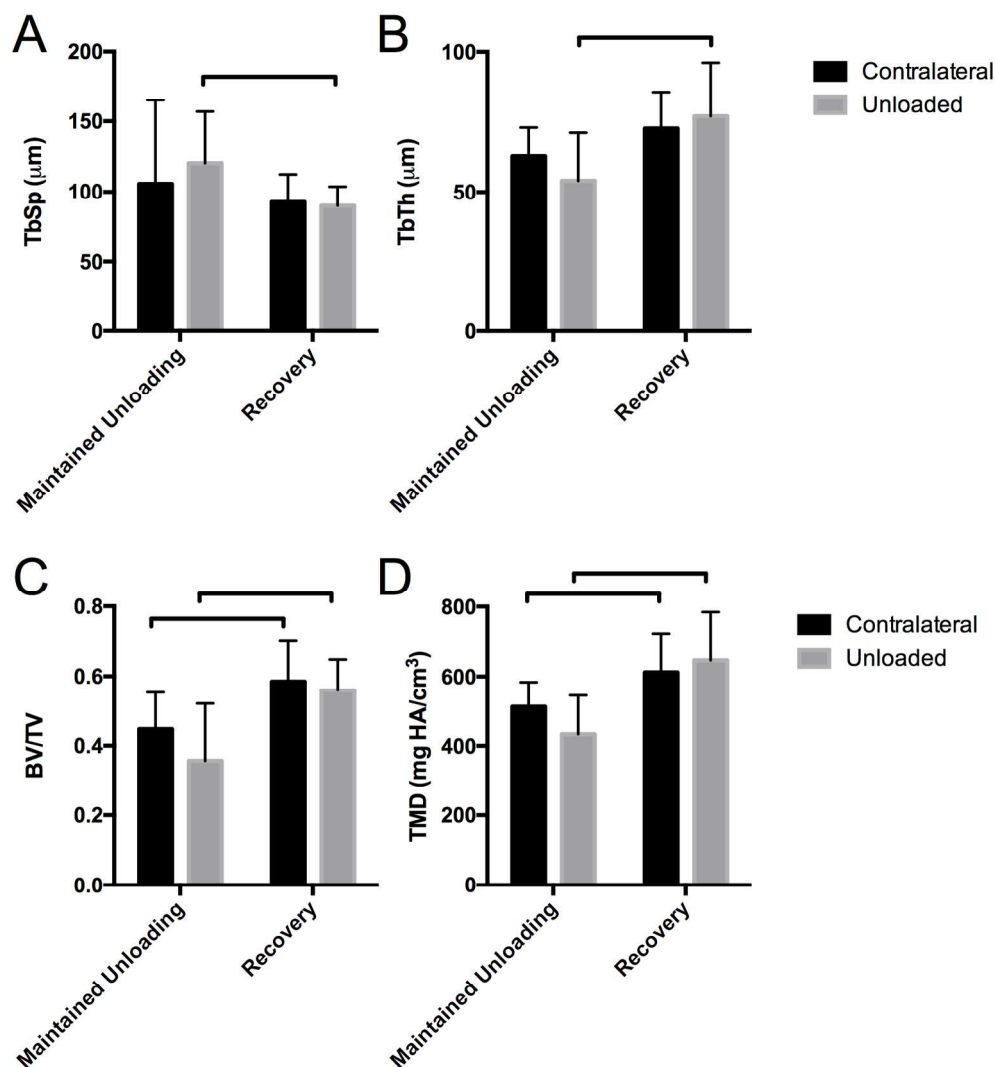536x374mm (144 x 144 DPI)

Figure 4. Recovery of bone morphometry after 2 weeks of postnatal Gluteal-target unloading, compared to Maintained Unloading, at P56. (A) TbSp was significantly lower and (B) TbTh was significantly higher for hips that were allowed to recover from postnatal unloading compared to Maintained Unloading. (C and D) Contralateral and Unloaded hips demonstrated higher BV/TV and TMD following a period of Recovery compared to Maintained Unloading. Bar indicates significant difference between group ($p < 0.05$). 361x390mm (144 x 144 DPI)
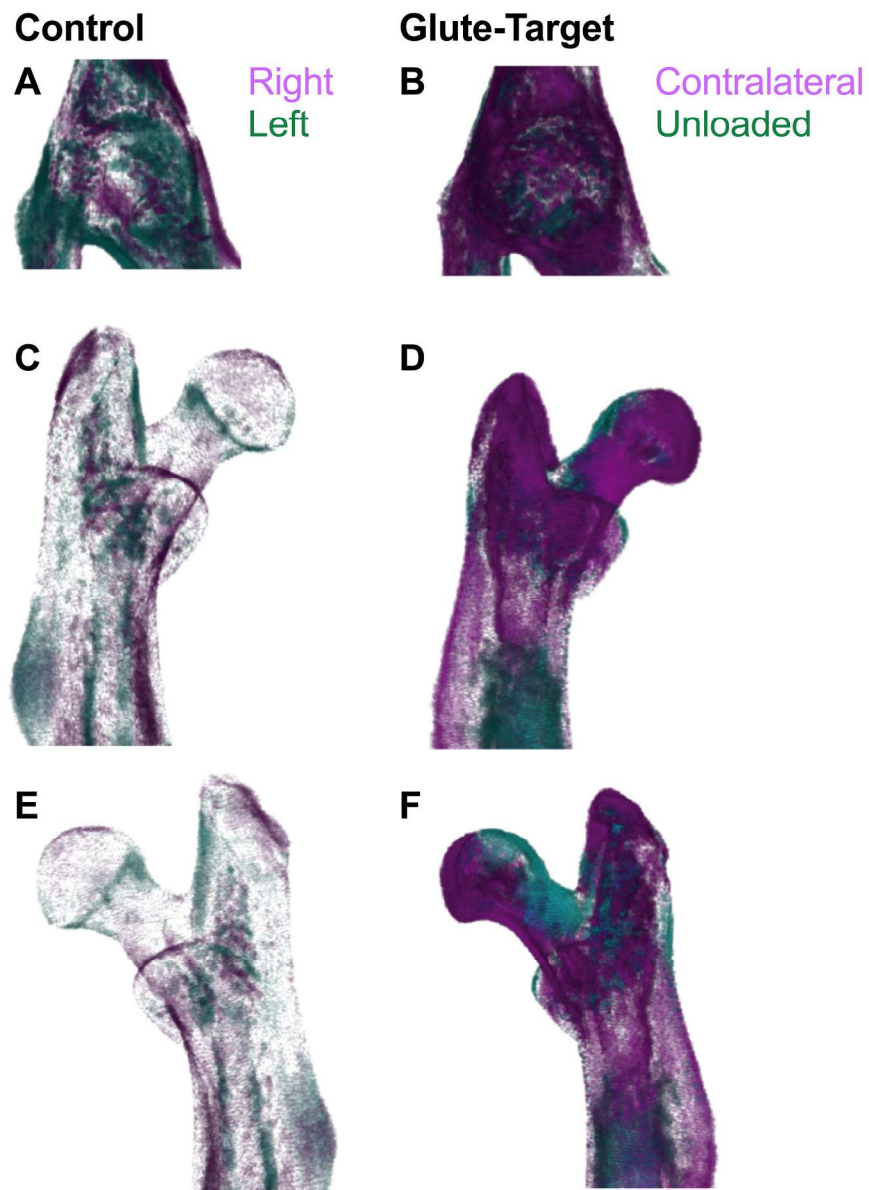
Figure 5. Shape comparisons using image registered atlases from microCT images of the (A & B) acetabulum, (C & D) posterior view of the proximal femur, and (E & F) anterior view of the proximal femur at P56. Right (magenta) and Left (turquoise) control hip overlay registrations are shown in A, C, and E; Contralateral (magenta) and Unloaded (turquoise) hip overlay registrations are shown in B, D, and F. Magenta pixels show localization where the contralateral/right atlas is larger, whereas turquoise pixels represent localization of a larger unloaded/left atlas.
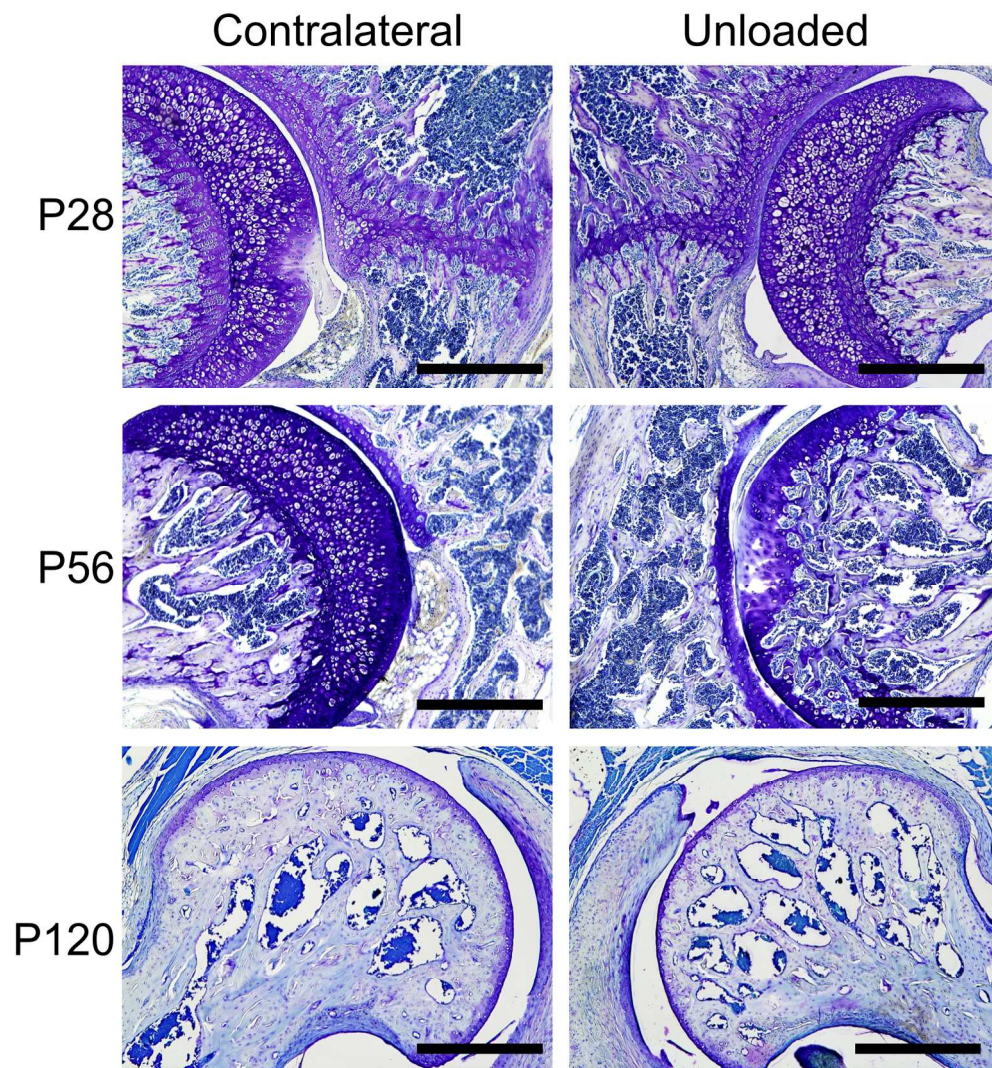226x306mm (300 x 300 DPI)

Figure 6. Histological sections stained with toluidine blue for P28, P56, and P120 contralateral and unloaded hips from the Glute-target group. Note the reduced femoral head size for the unloaded group at all 3 time points. Additionally, thickness of the triradiate cartilage is smaller for P28 unloaded hips compared to contralateral hips, and fusion of the femoral physis is accelerated for P56 unloaded hips compared to contralateral hips. Scale bar = 500micrometer.
361x390mm (144 x 144 DPI)

ARRIVE

The ARRIVE Guidelines Checklist
Animal Research: Reporting In Vivo Experiments

Carol Kilkenny[1], William J Browne[2], Innes C Cuthill[3], Michael Emerson[4] and Douglas G Altman[5]

[1]The National Centre for the Replacement, Refinement and Reduction of Animals in Research, London, UK, [2]School of Veterinary Science, University of Bristol, Bristol, UK, [3]School of Biological Sciences, University of Bristol, Bristol, UK, [4]National Heart and Lung Institute, Imperial College London, UK, [5]Centre for Statistics in Medicine, University of Oxford, Oxford, UK.

	ITEM	RECOMMENDATION	Section/ Paragraph
Title	1	Provide as accurate and concise a description of the content of the article as possible.	Pg 1
Abstract	2	Provide an accurate summary of the background, research objectives, including details of the species or strain of animal used, key methods, principal findings and conclusions of the study.	Page 2
INTRODUCTION			
Background	3	a. Include sufficient scientific background (including relevant references to previous work) to understand the motivation and context for the study, and explain the experimental approach and rationale. b. Explain how and why the animal species and model being used can address the scientific objectives and, where appropriate, the study's relevance to human biology.	Page 3-4, lines 24-63
Objectives	4	Clearly describe the primary and any secondary objectives of the study, or specific hypotheses being tested.	Page 3- Pg57-63
METHODS			
Ethical statement	5	Indicate the nature of the ethical review permissions, relevant licences (e.g. Animal [Scientific Procedures] Act 1986), and national or institutional guidelines for the care and use of animals, that cover the research.	Page 4, lines 66-67
Study design	6	For each experiment, give brief details of the study design including: a. The number of experimental and control groups. b. Any steps taken to minimise the effects of subjective bias when allocating animals to treatment (e.g. randomisation procedure) and when assessing results (e.g. if done, describe who was blinded and when). c. The experimental unit (e.g. a single animal, group or cage of animals). A time-line diagram or flow chart can be useful to illustrate how complex study designs were carried out.	Page 4-6 lines 66-123
Experimental procedures	7	For each experiment and each experimental group, including controls, provide precise details of all procedures carried out. For example: a. How (e.g. drug formulation and dose, site and route of administration, anaesthesia and analgesia used [including monitoring], surgical procedure, method of euthanasia). Provide details of any specialist equipment used, including supplier(s). b. When (e.g. time of day). c. Where (e.g. home cage, laboratory, water maze). d. Why (e.g. rationale for choice of specific anaesthetic, route of administration, drug dose used).	Page 4-6 lines 66-123
Experimental animals	8	a. Provide details of the animals used, including species, strain, sex, developmental stage (e.g. mean or median age plus age range) and weight (e.g. mean or median weight plus weight range). b. Provide further relevant information such as the source of animals, international strain nomenclature, genetic modification status (e.g. knock-out or transgenic), genotype, health/immune status, drug or test naïve, previous procedures, etc.	Page 4-5, lines 67-68

Housing and husbandry	9	Provide details of: a. Housing (type of facility e.g. specific pathogen free [SPF]; type of cage or housing; bedding material; number of cage companions; tank shape and material etc. for fish). b. Husbandry conditions (e.g. breeding programme, light/dark cycle, temperature, quality of water etc for fish, type of food, access to food and water, environmental enrichment). c. Welfare-related assessments and interventions that were carried out prior to, during, or after the experiment.	Line 75-78
Sample size	10	a. Specify the total number of animals used in each experiment, and the number of animals in each experimental group. b. Explain how the number of animals was arrived at. Provide details of any sample size calculation used. c. Indicate the number of independent replications of each experiment, if relevant.	Line 67, Line 75
Allocating animals to experimental groups	11	a. Give full details of how animals were allocated to experimental groups, including randomisation or matching if done. b. Describe the order in which the animals in the different experimental groups were treated and assessed.	Lines 67-75
Experimental outcomes	12	Clearly define the primary and secondary experimental outcomes assessed (e.g. cell death, molecular markers, behavioural changes).	Lines 81-117
Statistical methods	13	a. Provide details of the statistical methods used for each analysis. b. Specify the unit of analysis for each dataset (e.g. single animal, group of animals, single neuron). c. Describe any methods used to assess whether the data met the assumptions of the statistical approach.	lines 119-125
RESULTS			
Baseline data	14	For each experimental group, report relevant characteristics and health status of animals (e.g. weight, microbiological status, and drug or test naïve) prior to treatment or testing. (This information can often be tabulated).	Lines 127-132
Numbers analysed	15	a. Report the number of animals in each group included in each analysis. Report absolute numbers (e.g. 10/20, not 50%^{2}). b. If any animals or data were not included in the analysis, explain why.	Line 127
Outcomes and estimation	16	Report the results for each analysis carried out, with a measure of precision (e.g. standard error or confidence interval).	Line 127-180
Adverse events	17	a. Give details of all important adverse events in each experimental group. b. Describe any modifications to the experimental protocols made to reduce adverse events.	none
DISCUSSION			
Interpretation/ scientific implications	18	a. Interpret the results, taking into account the study objectives and hypotheses, current theory and other relevant studies in the literature. b. Comment on the study limitations including any potential sources of bias, any limitations of the animal model, and the imprecision associated with the results[2]. c. Describe any implications of your experimental methods or findings for the replacement, refinement or reduction (the 3Rs) of the use of animals in research.	Lines 182-242
Generalisability/ translation	19	Comment on whether, and how, the findings of this study are likely to translate to other species or systems, including any relevance to human biology.	Lines 235-242
Funding	20	List all funding sources (including grant number) and the role of the funder(s) in the study.	244-250

NC 3Rs

References:
1. Kilkenny C, Browne WJ, Cuthill IC, Emerson M, Altman DG (2010) Improving Bioscience Research Reporting: The ARRIVE Guidelines for Reporting Animal Research. *PLoS Biol* 8(6): e1000412. doi:10.1371/journal.pbio.1000412
2. Schulz KF, Altman DG, Moher D, the CONSORT Group (2010) CONSORT 2010 Statement: updated guidelines for reporting parallel group randomised trials. *BMJ* 340:c332.